HiSST: 3rd International Conference on
High-Speed Vehicle Science & Technology

14–19 April 2024, Busan, Korea

Eliminating Atomic Oxygen from RST Nozzle Simulations

Tristan Vanyai[1], *Nicholas N. Gibbons*[1]

Abstract

Correctly simulating the chemical composition in a test flow is a critical element of supersonic combustion experiments. Radicals generated in the stagnation region of a reflected shock tunnel could be seen as a key departure from the flow in flight experiments. However, there is evidence that only considering 5 chemical species in air gas models is artificially inflating the inferred concentration of atomic oxygen, O, in these test flows. By including a 6th species, NO_2, the concentration of O is decreased by many orders of magnitude at conditions suitable for testing supersonic combustors. This paper presents comparisons between 5- and 6-species air schemes for simulations of nozzles and subsequent combustion experiments, that indicate the importance of including NO_2 in reflected shock tunnel nozzle simulations.

Keywords: *Hypersonics, Combustion, Ground-Testing*

Nomenclature

p	Pressure (Pa)	HC	High Compression (side)
T	Temperature (K)	LC	Low Compression (side)
v	Velocity (m/s)	RST	Reflected Shock Tunnel
Y	Mass fraction	stag	Stagnation (nozzle supply)
CL	Centreline		

1. Introduction

Consider a reflected shock tunnel (RST), such as T4 at The University of Queensland [1], shown in Fig. 1. The purpose of all items upstream of the nozzle (to the left on Fig. 1) is to produce a high pressure, high temperature stagnation region. Pressures and temperatures in the stagnation region typically range from 1 MPa to 100 MPa and 1500 K to 6000 K, respectively. At these stagnation conditions, air molecules (primarily N_2 and O_2) dissociate into a chemical equilibrium of multiple important molecules, atoms and radicals, primarily N, O, NO, NO_2, N_2O and O_3.

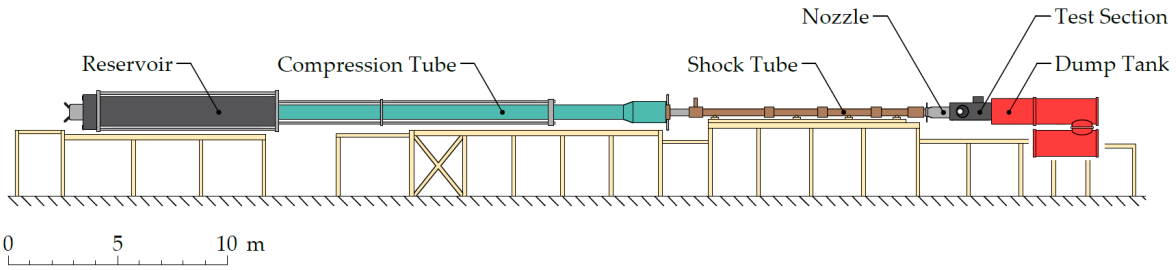

Fig 1. The T4 Reflected Shock Tunnel, from [2].

[1] *School of Mechanical and Mining Engineering, The University of Queensland, St. Lucia QLD 4072, Australia*

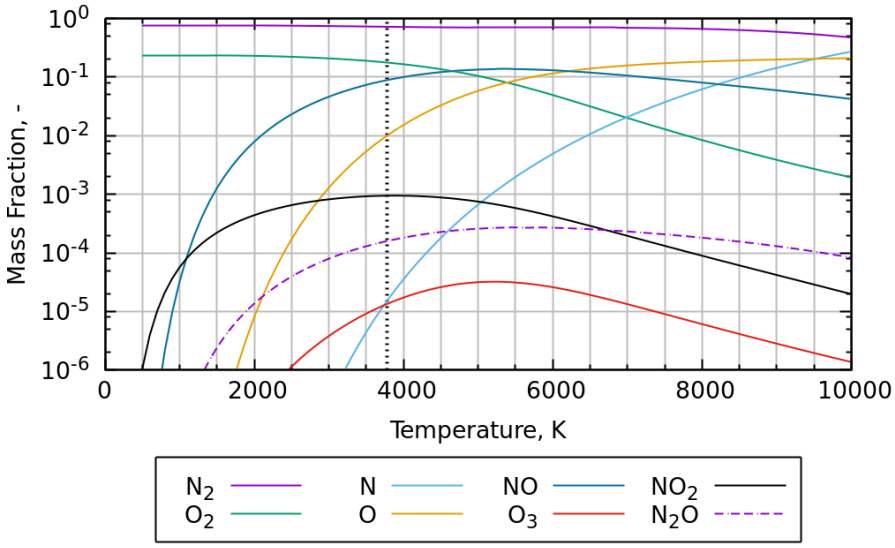

Fig 2. Equilibrium chemical composition at 44 MPa, from [3].

A typical Mach 10 flight-equivalent condition from [4] requires a stagnation temperature of 3770 K and a stagnation pressure of 44 MPa. Figure 2 shows the chemical equilibrium composition calculated using the NASA CEA program [5] at this pressure for an appropriate range of temperatures, with the Mach 10 enthalpy condition indicated as a dashed line. At temperatures around this condition at 44 MPa, Fig. 2 shows that the stagnation region primarily consists of molecular species N_2 and O_2, with a considerable amount of the NO radical of the order 10 %. Atomic oxygen, O, is also present at around 1 %, followed by a small amount of NO_2 at approximately 0.1 %. Other species such as N_2O and O_3 are less abundant, and won't be considered further in this paper.

Of course, the equilibrium scenario in the stagnation region is not the full story; this gas is accelerated through a nozzle before reaching experimental models in the test section. Here is where the treatment of chemical composition gets interesting, because the flow rapidly expands and cools down as it traverses the nozzle, undergoing a degree of "chemical freezing", and trapping radicals in the flow. There is no longer high pressure for chemical reactions to take place and reach equilibrium, thus finite chemistry effects must be considered. And this is a problem, as we do not have chemical reaction schemes tuned for these temperatures, pressures and species.

Traditionally, the Gupta et al. scheme [6] is used to model reactions in RST nozzles. Given the temperatures and pressures considered here, we can ignore ionisation effects, leaving us with the 5 chemical species: N_2, O_2, N, O and NO. We will thus refer to this scheme as the 5-species scheme, the equations for which are given in Eqs. (1) to (6). Reaction rate coefficients can be found in [6].

$$O_2 + M \rightleftharpoons 2\,O + M \tag{1}$$

$$N_2 + M \rightleftharpoons 2\,N + M \tag{2}$$

$$N_2 + N \rightleftharpoons 2\,N + N \tag{3}$$

$$NO + M \rightleftharpoons N + O + M \tag{4}$$

$$NO + O \rightleftharpoons O_2 + N \tag{5}$$

$$N_2 + O \rightleftharpoons NO + N \tag{6}$$

Examining Eqs. (1) to (6), we note our oxygen atoms are constrained to only three species: O_2, O and NO. Since oxygen dissociates more readily than nitrogen, there is typically a larger concentration of free

O, and small levels of N, as indicated by Fig. 2. The only way dissociated oxygen can recombine in the 5-species scheme is to form NO, which requires an equal amount of dissociated nitrogen. As such, there will always be an overabundance of O. We note that this is a relatively simplistic way of considering the complex reaction scheme, given that O can react directly with N_2 in Eq. (6), however this consideration does serve as an intuitive motivator to consider more complex reaction schemes.

The next step is to consider a 6-species reaction scheme, produced by removing all hydrogen-containing molecules in the Jachimowski 1992 combustion scheme [7]. This leaves us with N_2, O_2, N, O, NO and, crucially, NO_2, per Eqs. (7) to (12). Reaction rate coefficients can be found in [7]. Consideration of the NO_2 molecule allows spare O atoms to recombine with NO and form NO_2, eliminating the over-constraining nature of the 5-species scheme. We consider the inclusion of NO_2 to be critical, as it allows a pathway to consume excess dissociated O.

$$2\,O + M \rightleftharpoons O_2 + M \tag{7}$$

$$2\,N + M \rightleftharpoons N_2 + M \tag{8}$$

$$N + O_2 \rightleftharpoons NO + O \tag{9}$$

$$N + NO \rightleftharpoons N_2 + O \tag{10}$$

$$O + NO_2 \rightleftharpoons NO + O_2 \tag{11}$$

$$M + NO_2 \rightleftharpoons NO + O + M \tag{12}$$

2. Ignition Delay Vitiation Study

The concentration of O in RST test flows has a remarkable influence on numerical simulation of combustion experiments. A vitiation study was performed using the Gas Dynamic Toolkit (GDTk) [8], examining combustion within a constant volume (constant density) reactor, using the Jachimowski reaction scheme [7]. Pressure was initially set at 1 atmosphere, and the initial temperature was varied from 1000 K to 1500 K for different tests, representing typical entrance conditions of a supersonic combustor. The initial chemical composition was set as a stoichiometric hydrogen-air mixture in addition to increasing levels of atomic oxygen. Ignition delay was defined as the simulation time to reach a hydroxyl molar concentration of $X_{OH} = 5.0 \times 10^{-3}$.

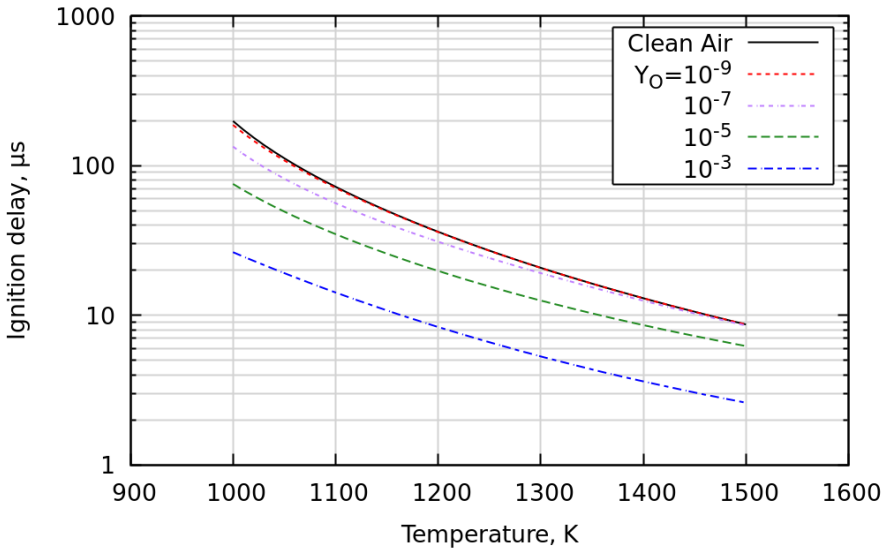

Fig 3. Ignition delay of a stoichiometric air-hydrogen mixture at $p = 1$ atm.

Figure 3 shows the resulting ignition delays for different O mass fractions as the initial temperature is varied. It is clear that O can significantly reduce ignition delay even at mass fractions as low as $Y_O = 10^{-7}$. At 1000 K, a mass fraction of $Y_O = 10^{-3}$ reduces the ignition delay from 198.3 µs to 26.4 µs. For a typical combustor flow velocity of 2500 m s^{-1}, this corresponds to a reduction of ignition length from 496 mm to 66 mm. We can therefore expect that supersonic combustion experiments will be affected by the concentration of atomic oxygen in the freestream of RST test flows. The next step is thus to examine how these RST nozzle flows are affected by our different reaction schemes.

3. RST Nozzle Simulations

Non-equilibrium nozzle calculations are a critical part of analysing the data collected from a reflected shock tunnel, since the test flow itself is not actually measured during the experiments. In this section we consider a sweep of nozzle calculations to compare the effects of 5- and 6-species gas models, using two simulation tools from the Gas-Dynamic Toolkit (GDTk) [8]. The first is a quasi-one-dimensional simulator called NENZF1d, a production tool for experimenters which generates flow conditions very quickly while still accounting for chemical and thermal nonequilibrium. NENZF1d is used to sweep over a wide range of conditions, parameterised by their stagnation temperature and stagnation pressure.

Secondly, these results have been spot checked by a handful of 2D axisymmetric simulations, which are more expensive but can account for viscous effects and the actual shape of the nozzle geometry, performed using the computational fluid dynamics code Eilmer [9]. Eilmer is an open-source finite-volume compressible flow solver developed for high-speed and hypersonic flow research, with a Jacobian-Free Newton-Krylov (JFNK) method for rapidly solving the steady-state condition of a flow problem [10]. Details of these calculations are provided in figure 4, which also shows an example nozzle outflow produced using a nominal (180x72) and fine (360x120) grid.

Eilmer Solver Settings

Solver Mode:	2D Axisymmetric
Temporal Advancement:	JFNK Steady-State
Reconstruction:	3rd Order Structured
Turbulence Model:	1 Eqn. Spalart-Allmaras
Transition Point:	+100 mm downstream of throat
Limiter Smoothing:	1×10^{-6}
Flux Calculator:	AUSMDV

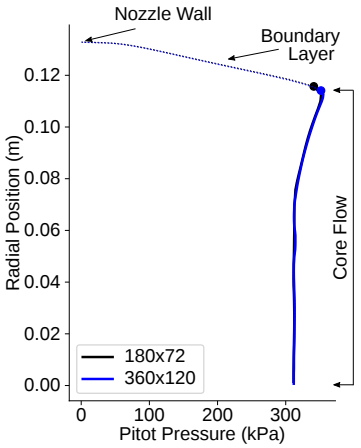

Fig 4. Left: Table of solver parameters used for Eilmer nozzle calculations. Right: Example output pitot pressure, showing grid convergence and region of core flow.

Nominal Mach 4 and Mach 8 nozzles were simulated, however for brevity only the Mach 8 nozzles will be presented here. Test gas compositions extracted from both sets of calculations are shown in Fig. 5. Continuous lines show output from NENZF1d, whilst discrete points mark the averaged core flow from the Eilmer axisymmetric nozzle simulations. As shown in Fig. 5, there is excellent agreement between axisymmetric Eilmer simulations and corresponding NENZF1d results.

As stagnation temperature is increased, the dissociation of nitrogen and oxygen increases as expected. This is exacerbated at low pressures, where chemical freezing is expected to be more prominent. I.e. as stagnation pressure is increased, chemical reaction rates increase, and flow passing through the RST nozzle more rapidly approaches the low-temperature equilibrium composition. At sufficiently high pressures and sufficiently long nozzles, one would expect the chemistry to eventually reach chemical equilibrium at the RST nozzle exhaust.

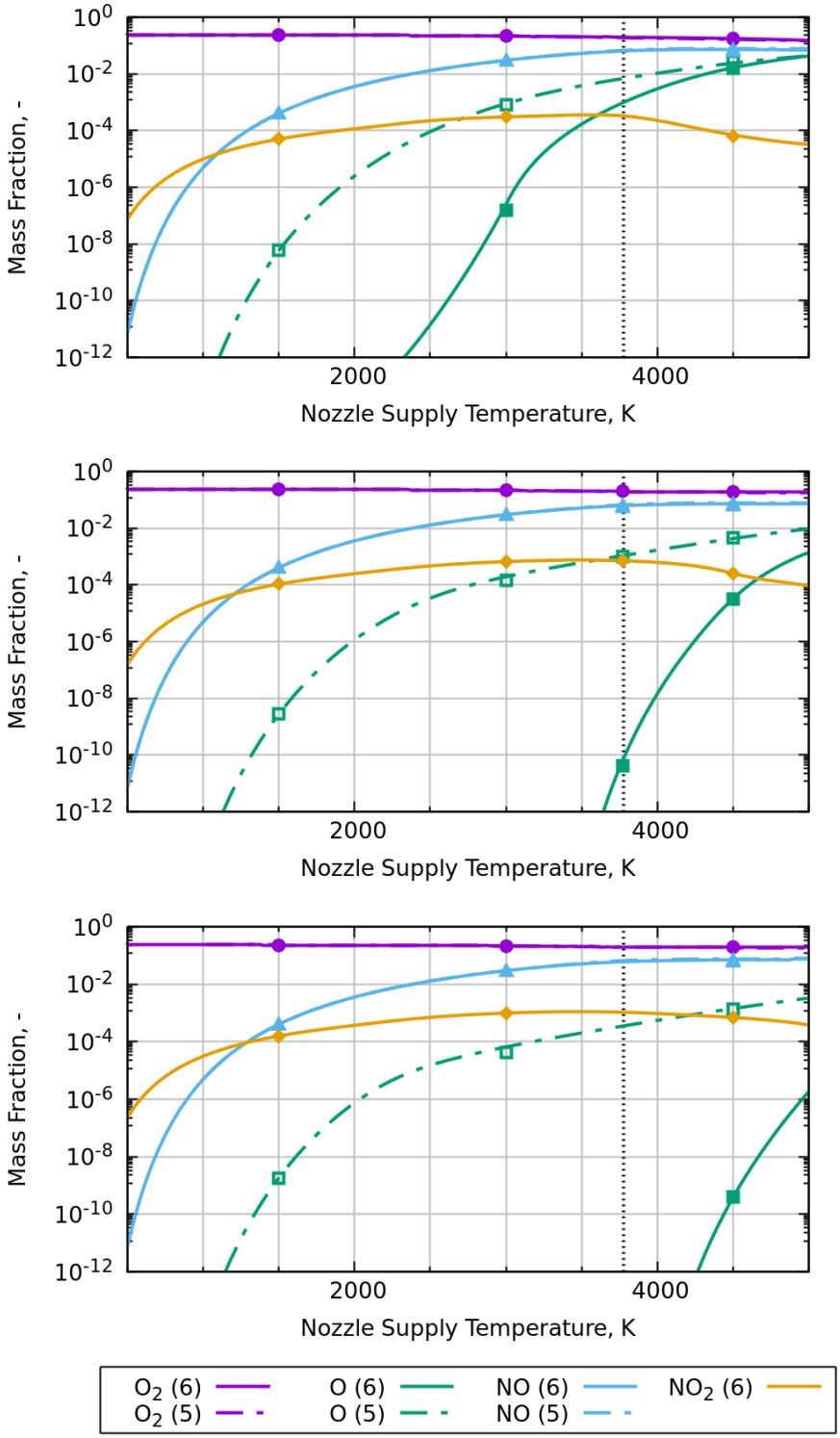

Fig 5. Variation in test flow (RST nozzle exhaust) composition at 10 MPa (top), 45 MPa (middle) and 100 MPa (bottom).

In general, there is excellent agreement between 5-species (solid) and 6-species (dashed) reaction schemes for all species except O. For all cases, and primarily for high-pressure, middling temperature cases, Y_O is considerably affected by the change to the 6-species reaction scheme. With the introduction of NO_2, O is effectively eliminated except at low pressure, high temperature conditions. Particularly at the Mach 10 condition indicated by the dashed line at $T_{stag} = 3770$ K and $p_{stag} = 45$ MPa, atomic oxygen has been reduced from $Y_O = 10^{-3}$ to $Y_O = 4 \times 10^{-11}$. Recalling Fig. 3, we note that this will have significant impact on simulated ignition delay. We note in Fig. 5 that NO quickly becomes significant at temperatures above approximately 2000 K, and is of the order of 1 % to 10 %. This seems to be almost independent of pressure and reaction scheme.

We thus conclude that selection of reaction scheme and allowed reactants is crucial to correctly determine the chemical composition of RST nozzle test flow. However, how does this affect combustion within RST experimental models? In the next section, we examine CFD combustion simulations with different test flow compositions.

4. Combustion simulations of RST experiments

We have performed a series of numerical simulations of the thermal compression scramjet geometry from [4]. The experimental model geometry is shown in Fig. 6, with a constant width of 75 mm. Hydrogen fuel was injected from cylindrical injectors within the inlet, 94 mm downstream of the entrance plane, at a nominal equivalence ratio of ER = 0.8.

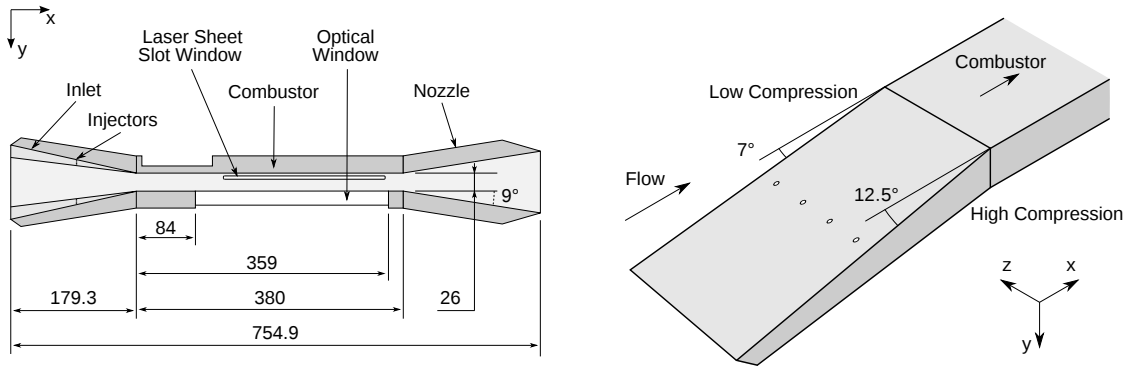

(a) Engine geometry, dimensions in mm

(b) Detailed view of non-uniform intake, 3D intake

Fig 6. Scramjet model geometry. Flow travels along the positive x-axis, from [4].

Simulations were conducted using US3D [11], a general-purpose compressible flow solver for hybrid structured/unstructured grids on complex geometries. US3D solves the compressible Reynolds Averaged Navier-Stokes equations, supplemented with the Spalart-Allmaras one-equation turbulence model, and a series of scalar transport equations for a number of chemical species. Chemical reactions are modelled using the 13-species, 33-equation scheme of Jachimowski [7], and the inviscid fluxes were computed using a Modified Steger-Warming method discussed in [11]. Time advancement is performed using the implicit Full-Matrix Point Relaxation method from [12], which solves the large sparse linear system associated with each timestep using a series of substeps that sweep across the domain. Each sweep uses the off-diagonal values of the previous sweep, which allows the matrix to be solved in parallel across thousands of processors efficiently. This parallelism is handled using an automated block decomposition affected by Parmetis, which splits a initial large mesh of hexahedral elements into unstructured blocks, each of which is assigned to a single processor. US3D has been used for many successful simulations of reacting supersonic flowpaths, including [13], and this work uses the same settings and parameters as described in previous studies.

The inflow boundary condition located at $x = -180$ mm was varied to examine the effect of considering different reaction schemes within the nozzle simulations. The experiment stagnation pressure and shock

speed were measured for each test, and then averaged over the entire experimental campaign (for one specific test condition). These values were used as the inputs at the RST nozzle throat and full, axisymmetric nozzle simulations were run using Eilmer with both 5-species and 6-species chemical reaction schemes. The resulting core flow outputs (corresponding to the model intake area, $r < 60$ mm [14]) are shown in Table 1 alongside a "Clean air" solution, consisting of the 5-species thermodynamic properties, but replacing the composition with only N_2 and O_2.

Table 1. RST nozzle exhaust/simulation inflow boundary condition.

	Clean air	5-Species	6-Species
ρ (kg/m^{-3})	0.0358	0.0358	0.0356
T (K)	405	405	412
v (m/s)	2936	2936	2946
Y_{N_2}	0.77	0.7349	0.7378
Y_{O_2}	0.23	0.1960	0.2000
Y_N	0.0	0.0	0.0
Y_O	0.0	1.03×10^{-3}	5.11×10^{-12}
Y_{NO}	0.0	6.81×10^{-2}	6.15×10^{-2}
Y_{NO_2}	0.0	0.0	7.13×10^{-4}

The pressure traces from these 3D simulations are shown in Fig. 7. As the flow through the model is non-uniform, pressure data was taken not only along the centreline (CL) but also along low compression (LC) and high compression (HC) sides, see Fig. 6b. The spanwise locations of these traces are $z = 18.75$ mm, 37.50 mm, and 56.25 mm for the HC, CL and LC sides, respectively. Figure 7 shows pressure data from experimental test 11776, alongside the three sets of numerical data. As we are focusing on comparisons between numerical simulations, experimental error bars have not been included in Figure 7. Measurement uncertainty on an individual pressure transducer is of the order 1 % to 5 %, with further estimates of uncertainty from aggregate data sets being presented in [4, 14].

The difference between 5-species and 6-species simulations in Fig. 7 is stark. 5-species inflow with $Y_O = 0.1$ % predicts significant combustion-induced pressure rise 100 mm into the combustor, with pressure immediately reaching a plateau, and only minor increases in pressure downstream as the fuel and air continue to combust in a mixing-limited manner. Conversely, the 6-species mechanism closely matches the clean air scenario, and is closer to matching the experimental data. In these solutions, combustion-induced pressure rises occur some 100 mm to 200 mm further downstream than the 5-species solution, and increase over a much longer streamwise distance. Whilst the match between the experimental pressure data and the 6-species/clean air solutions is certainly not perfect, particularly on the HC side towards the end of the combustor, in general the 6-species pressure trends agree better than in the 5-species simulation.

We now examine the mixing and combustion efficiencies in Fig. 8. The combustion efficiency is how much fuel has burned (how much heat has been released); the entrainment efficiency is how much all fuel and air species have mixed; whilst the mixing efficiency is how much initial reactants H_2 and O_2 are mixed and ready to burn, but limited by finite-rate chemistry. Further descriptions and mathematical definitions are found on page 96 of [15].

Entrainment efficiencies show very similar trends for all reaction schemes, however we do note the increase for the clean air case. Looking at Fig. 7, we would expect 6-species and clean air to agree better, so it is possible the increased N_2 (which is not included in calculating entrainment efficiency) in the clean air case is affecting the normalisation of the entrainment efficiency. However, the difference for 5-species combustion and mixing efficiency tells a very strong story. The different schemes all agree until the beginning of the combustor at $x = 0$ m, as the hydrogen fuel mixes with the freestream air. Upon entering the higher pressure in the combustor, combustion begins immediately for the 5-species

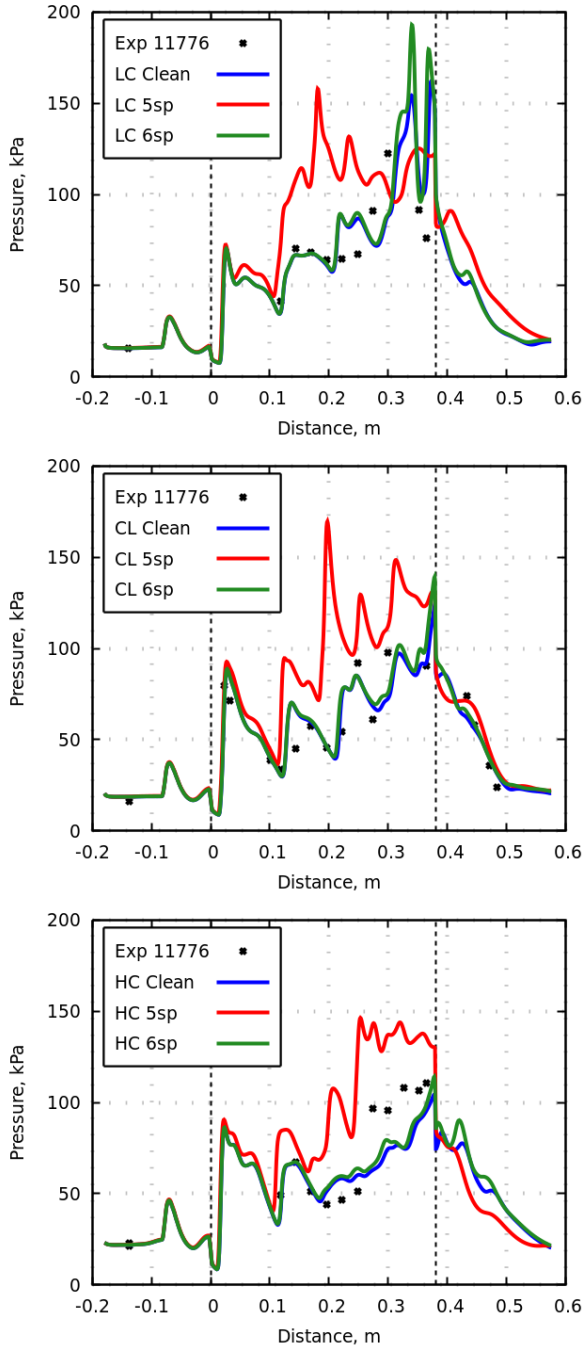

Fig 7. Comparisons of pressure in the engine along the LC side (top), Centreline (middle) and HC Side (bottom).

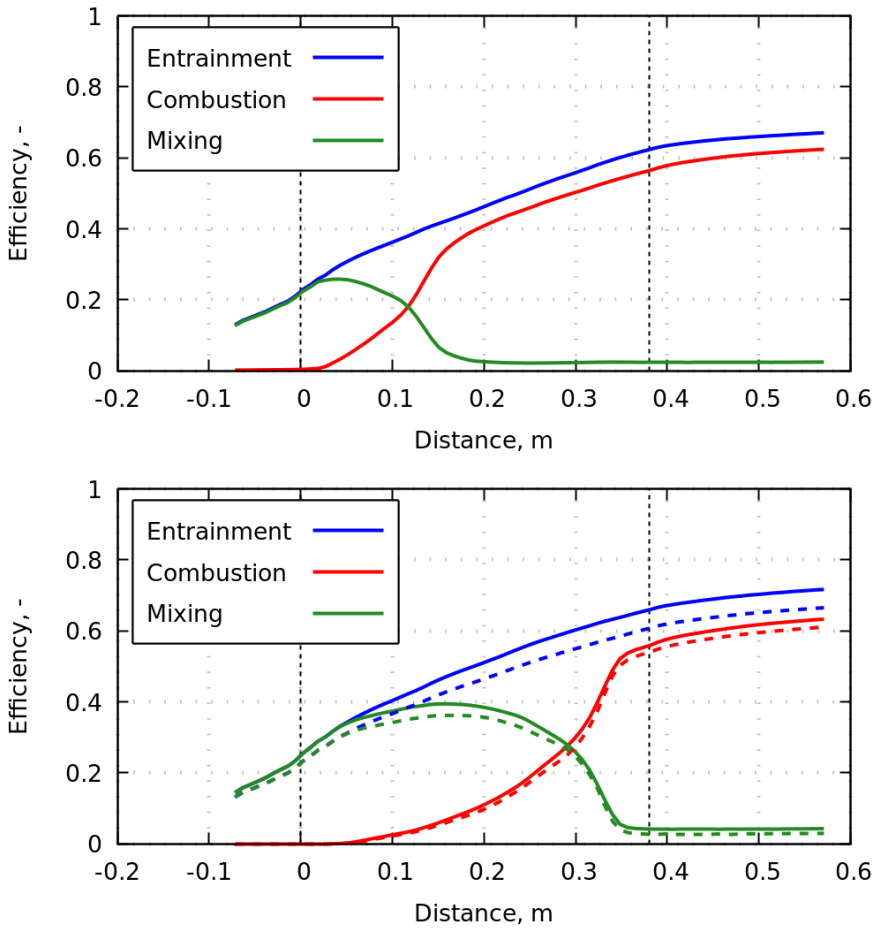

Fig 8. Mixing and combustion efficiencies for 5-species inflow (top), and both clean air (solid) and 6-species (dashed) inflows (bottom).

case, with the flow becoming reaction-limited by approximately $x = 0.15$ m. On the other hand, the 6-species and clean air schemes exhibit similar reaction lengths, occurring over the entire length of the combustor. Given combustor pressures and temperatures of approximately 50 kPa and 1200 K to 1500 K, respectively, we expect combined Pergament ignition and reaction lengths [16] of approximately 0.2 m to 0.3 m (also see [17] for more discussion on combustion lengths), agreeing with 6-species, clean air and experimental data rather than the 5-species simulations.

It is clearly the choice of reaction scheme in the nozzle having this dramatic effect on combustion in these simulations. However, let us confirm that it is the atomic oxygen making this difference, and that it remains in high concentration, remembering that at high pressure the oxygen should recombine. Figure 9 shows the conversion of atomic oxygen to nitrogen dioxide along the centreline of the symmetry plane ($y = 13$ mm above the combustor floor). There is clearly a disconnect between the 5-species reaction scheme in the RST nozzle simulation and the full Jachimowski combustion scheme within the scramjet simulation. O is consumed exponentially within the inlet and converted into NO_2, which increases to a value similar to the 6-species RST nozzle exhaust value at approximately 0.1 %. However, we note that O is still of order $Y_O = 1 \times 10^{-4}$ at the combustor entrance, and never drops below 10^{-5}. Looking back to Fig. 3, we expect a significant decrease in ignition length, likely by 50 % or more. We thus conclude that the increase in atomic oxygen due to the 5-species reaction scheme in the RST nozzle has significantly reduced the ignition length, causing increased combustion efficiency and subsequent pressure rise to occur much further upstream in the simulations than occurred for the other schemes, or in experiments.

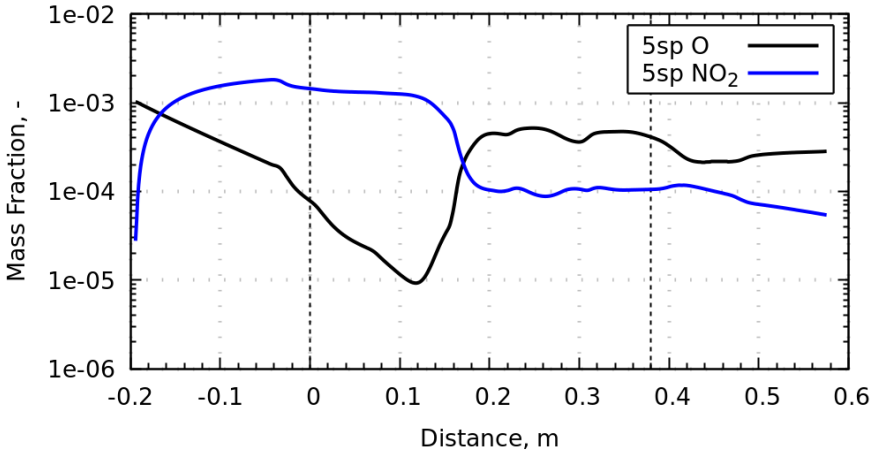

Fig 9. Consumption of O and production of NO_2 within the inlet of the 5-species inflow case.

5. Conclusions and future work

The presence of atomic oxygen in the test flows of reflected shock tunnels can significantly influence the results of combustion experiments. This paper presents evidence that there are lower values of atomic oxygen than predicted by the 5-species reaction scheme from Gupta et al. [6], indicating that RST experiments are even more representative of flight conditions than previously thought. This is especially true at high stagnation pressures, but potentially less true at excessively high temperatures above 4000 K, i.e. above Mach 10 flight conditions. A 6-species reaction scheme created by removing hydrogen species from Jachimowski's hydrogen-air combustion scheme produced numerical simulations that showed better agreement with both experimental and a clean air inflow condition. A key property of this scheme was the inclusion of NO_2 that allowed a new pathway to consume excess O. Ideally, future reaction schemes would be tuned to scramjet testing conditions, and include species such as NO_2, O_3 and N_2O.

References

[1] R. Stalker and R. Morgan, "The University of Queensland free piston shock tunnel T4 - Initial operation and preliminary calibration," in *Fourth National Space Engineering Symposium*, pp. 182–198, Institution of Engineers, Australia, 1988.

[2] L. J. Doherty, "An experimental investigation of an airframe integrated three-dimensional scramjet engine at a Mach 10 flight condition," PhD Thesis, The University of Queensland, Australia, 2014.

[3] T. Vanyai and N. Gibbons, "Atomic oxygen in supersonic combustion experiment inflows," in *The Australian Combustion Symposium 2021*, Australian Combustion Symposium, 2021.

[4] T. Vanyai, S. Brieschenk, M. Bricalli, T. Sopek, and T. J. McIntyre, "Thermal compression effects within a fundamental, hydrogen-fuelled scramjet," *Aerospace Science and Technology*, vol. 110, p. 106499, 2021.

[5] B. McBride and S. Gordon, *Computer Program for Calculation of Complex Chemical Equilibrium Compositions and Applications*. NASA Glenn Research Center, Cleveland, USA, June 1996. Reference publication 1311.

[6] R. N. Gupta, J. M. Yos, R. A. Thompson, and K.-P. Lee, "A review of reaction rates and thermodynamic and transport properties for an 11-species air model for chemical and thermal nonequilibrium calculations to 30000 k," tech. rep., NASA, 1990.

[7] C. J. Jachimowski, “An analysis of combustion studies in shock expansion tunnels and reflected shock tunnels,” Tech. Rep. TP-3224, NASA, 1992.

[8] R. J. Gollan, N. N. Gibbons, K. A. Damm, and P. Jacobs, “Gdtk: Gas dynamics toolkit.” https://gdtk.uqcloud.net/, 2023. Accessed: 08/03/24.

[9] N. N. Gibbons, K. A. Damm, P. A. Jacobs, and R. J. Gollan, “Eilmer: An open-source multi-physics hypersonic flow solver,” *Computer Physics Communications*, vol. 282, p. 108551, 2023.

[10] K. A. Damm, N. N. Gibbons, and R. Gollan, “Application of a jacobian-free newton-krylov method to the simulation of hypersonic flows,” in *AIAA SCITECH 2023 Forum*, no. 2023-2295, (National Harbor, MD & Online), January 2023.

[11] G. V. Candler, H. B. Johnson, I. Nompelis, V. M. Gidzak, P. K. Subbareddy, and M. Barnhardt, “Development of the us3d code for advanced compressible and reacting flow simulations,” in *53rd AIAA Aerospace Sciences Meeting*, p. 1893, 2015.

[12] M. Wright, G. Candler, and M. Prampolini, “Data-parallel lower-upper relaxation method for the navier-stokes equations,” *AIAA Journal*, vol. 34, pp. 1371–1377, July 1996.

[13] T. Vanyai, N. N. Gibbons, D. R. Curran, M. McGilvray, and V. Wheatley, “The effect of leading edge bluntness on scramjet performance,” *Aerospace Science and Technology*, vol. 146, p. 108907, 2024.

[14] T. Vanyai, “Experimental investigation of a 3D thermal compression scramjet using advanced optical techniques,” PhD Thesis, The University of Queensland, Australia, 2018.

[15] N. Gibbons, “Simulation and dynamics of hypersonic turbulent combustion,” PhD Thesis, The University of Queensland, 2019.

[16] H. Pergament, “Theoretical analysis of non-equilibrium hydrogen-air reactions in flow systems,” in *AIAA Paper 63113*, 1963.

[17] M. K. Smart, “How much compression should a scramjet inlet do?,” *AIAA Journal*, vol. 50, pp. 610–619, Mar. 2012.